Published in final edited form as:
Biomaterials. 2007 October ; 28(28): 4078–4090. doi:10.1016/j.biomaterials.2007.05.033.

Fabrication of Porous Ultra-Short Single-Walled Carbon Nanotube Nanocomposite Scaffolds for Bone Tissue Engineering

Xinfeng Shi[1,2], **Balaji Sitharaman**[1,2,3], **Quynh P. Pham**[1], **Feng Liang**[2,3], **Katherine Wu**[1], **W. Edward Billups**[2,3], **Lon J. Wilson**[2,3], and **Antonios G. Mikos**[1,2,*]

[1]Department of Bioengineering, Rice University, MS-142, Houston, Texas, 77251-1892

[2]The Richard E. Smalley Institute for Nanoscale Science and Technology, Rice University, MS-100, Houston, Texas, 77251-1892

[3]Department of Chemistry, Rice University, MS-60, Houston, Texas, 77251-1892

Abstract

We investigated the fabrication of highly porous scaffolds made of three different materials [poly(propylene fumarate (PPF) polymer, an ultra-short single-walled carbon nanotube (US-tube) nanocomposite, and a dodecylated US-tube (F-US-tube) nanocomposite] in order to evaluate the effects of material composition and porosity on scaffold pore structure, mechanical properties, and marrow stromal cell culture. All scaffolds were produced by a thermal-crosslinking particulate-leaching technique at specific porogen contents of 75, 80, 85, and 90 vol%. Scanning electron microcopy, microcomputed tomography, and mercury intrusion porosimetry were used to analyze the pore structures of scaffolds. The porogen content was found to dictate the porosity of scaffolds. There was no significant difference in porosity, pore size, and interconnectivity among the different materials for the same porogen fraction. Nearly 100% of the pore volume was interconnected through 20 μm or larger connections for all scaffolds. While interconnectivity through larger connections improved with higher porosity, compressive mechanical properties of scaffolds declined at the same time. However, the compressive modulus, offset yield strength, and compressive strength of F-US-tube nanocomposites were higher than or similar to the corresponding properties for the PPF polymer and US-tube nanocomposites for all the porosities examined. As for *in vitro* osteoconductivity, marrow stromal cells demonstrated equally good cell attachment and proliferation on all scaffolds made of different materials at each porosity. These results indicate that functionalized ultra-short single-walled carbon nanotube nanocomposite scaffolds with tunable porosity and mechanical properties hold great promise for bone tissue engineering applications.

INTRODUCTION

A scaffold is one of the key components in the tissue engineering paradigm in which it can function as a template to allow new tissue growth and also provide temporary structural

[*]*Corresponding Author*: Prof. Antonios G. Mikos Department of Bioengineering Rice University P.O. Box 1892, MS-142 Houston, TX 77251-1892 Phone: (713) 348-5355 Fax: (713) 348-4244 mikos@rice.edu.

support while serving as a delivery vehicle for cells and/or bioactive molecules [1, 2]. An ideal scaffold for bone tissue regeneration should possess mechanical properties similar to the bone tissue being replaced, good biocompatibility with surrounding tissue, large porosity and pore size, high pore interconnectivity for bone tissue ingrowth, and biodegradability such that it is gradually replaced by growing bone tissue [3]. Despite extensive research, no existing man-made scaffold can meet all these requirements. The development of novel biomaterials and scaffold fabrication techniques is critical for the success of bone tissue engineering.

Recently, a variety of nanocomposite materials made of poly(propylene fumarate) (PPF) and single-walled carbon nanotubes (SWNTs) have been explored for potential use as scaffold materials in our laboratory [4–6]. These nanocomposites are injectable, thermally-crosslinkable, and cytocompatible *in vitro*, making them promising biomaterials for bone tissue engineering. SWNTs, especially ultra short SWNTs (US-tubes), significantly reinforced PPF polymer, whose inferior mechanical properties often limit its use as a highly porous scaffold for load bearing applications. Chemical functionalization of SWNTs can improve their dispersion into PPF, augmenting their reinforcing effects [5]. Therefore, functionalized US-tubes (F-US-tubes) were introduced here to investigate their effects on scaffolds for bone tissue engineering.

In this study, we examined the scaffold fabrication process to generate three different materials: pure PPF polymer, US-tube/PPF nanocomposite, and F-US-tube/PPF nanocomposite. While scaffolds with a high porosity would allow bone tissue ingrowth, their mechanical properties could become compromised [7]. Therefore, scaffolds with porosities of 75, 80, 85, and 90 vol% were designed for this experiment. To our knowledge, few studies have produced a SWNT nanocomposite scaffold for bone tissue engineering and there has been little characterization of such highly porous scaffolds for their physical and biological properties [8–11]. We demonstrate here that up to 90 vol% scaffolds of nanocomposites can be reproducibly created via thermal-crosslinking and salt porogen leaching. Furthermore, we ask the following questions: (1) How do the carbon nanotubes affect the pore structure and mechanical properties of scaffolds? (2) What are the effects of different porosity on the pore structure and mechanical properties of scaffolds? (3) What are the responses of bone marrow stromal cells cultured on scaffolds made of different nanomaterials with varying porosity?

MATERIALS AND METHODS

Polymer Preparation

Poly(propylene fumarate) (PPF) and its crosslinking agent propylene fumarate-diacrylate (PF-DA) were synthesized as previously described [12, 13]. The PPF used in this study had a number average molecular weight (M_n) of 2660 and a polydispersity index of 2.1. PF-DA had a molecular weight of 340. All reagents and organic solvents were used as received. PPF and PF-DA were mixed at a 1:2.1 mass ratio prior to usage.

US-tube Synthesis and Functionalization

US-tubes were produced by fluorination followed by pyrolysis of as-received SWNTs as previously described [14]. The resulting nanotubes had lengths of 20–80 nm and were much shorter than SWNTs produced by a high pressure carbon monoxide (HiPco) process which are hundreds of nanometers to several microns in length [15]. US-tubes were then functionalized by an alkylation-based reduction [16]. Briefly, NH_3 (~60 mL) was condensed into a flame-dried 100 mL flask loaded with US-tubes (20 mg, 1.7 mmol of carbon). This was followed by the addition of sodium metal (184 mg, 8 mmol), and then 1-iodododecane

(1.9 g, 6.4 mmol). The reaction mixture was subsequently allowed to stir overnight with the slow evaporation of NH_3. The remaining mixture was diluted with ethanol (10 mL) and then with water (20 mL). After acidification with 10% HCl, the US-tubes were extracted into hexane (50 mL), and washed three times with water (50 mL each time). The final hexane layer was filtered through a 0.2 μm PTFE membrane filter, washed with ethanol (200 mL) and chloroform (200 mL), and then dried to give functionalized US-tubes (F-US-tubes, Figure 1). The functionalization was confirmed by the large disorder band (at ~1290 cm^{-1}) in the Raman spectra of F-US-tubes. The mass loss of F-US-tubes in thermogravimetric analysis (TGA, 10°C/min to 800 °C in argon) was 40 % indicating that one out of every 21 carbon atoms on the sidewalls of US-tubes was covalently attached with a dodecyl group [17].

Fabrication of Nanocomposites and Their Scaffolds

Following an established procedure of high shear mixing, sonicating and drying [5], the carbon nanotubes were uniformly distributed into the PPF/PF-DA mixture (subsequently referred to as PPF). US-tubes were loaded at 0.5 wt% concentration because US-tube/PPF nanocomposites achieved their maximum mechanical properties at this loading concentration [6]. F-US-tubes were loaded at 0.83 wt% concentration to provide the nanocomposite with the same amount of carbon nanotubes as the US-tube/PPF nanocomposite.

Porous scaffolds were fabricated by a thermal-crosslinking particulate-leaching technique with NaCl as the water soluble porogen [11]. PPF or the nanocomposites were first mixed with 1 wt% free-radical initiator, benzoyl peroxide, followed by the addition of the appropriate amount of NaCl (300–500 μm crystal size) sieved with USA Standard Testing Sieves (Fisher Scientific, Pittsburgh, PA). The mixtures were then cast and thermally crosslinked at 100 °C for 24 h in cylindrical Teflon molds (4 mm diameter and 8 mm height) or cylindrical glass molds (6.5 mm diameter). The 100 °C curing temperature was applied here to ensure complete crosslinking of the scaffold materials [18]. After being removed from the molds, the 4 × 8 mm samples were used for the characterizations of pore structure and mechanical properties and the 6.5 mm-diameter samples were cut into 2 mm thick discs for cell seeding. Finally, all crosslinked samples were soaked in water (water was changed every 8 h) on a shaker table (80 rpm) at room temperature for 3 days to leach out the NaCl porogen. Afterwards, they were blotted with absorbent paper and then vacuum dried for 24 h.

The amount of NaCl used to generate 75, 80, 85, and 90 vol% porous scaffolds was calculated according to the following equations:

$$\varepsilon = \frac{V_{NaCl}}{V_{NaCl} + V_{Nano}} \times 100\% \quad (1)$$

$$W_{NaCl} = \frac{\varepsilon}{1-\varepsilon} \times \frac{\rho_{NaCl}}{\rho_{Nano}} \times W_{Nano} \quad (2)$$

Where ε is the apparent porosity (volume percent of porogen in a scaffold), V_{NaCl} and V_{Nano} are the volumes of NaCl and the nanocomposite in a scaffold, W_{NaCl} and W_{Nano} are the weights of NaCl and the nanocomposite in a scaffold, and ρ_{NaCl} is the density of NaCl (2.17 g/mL). The density of the nanocomposite (ρ_{Nano}) was calculated by measuring the mass and volume of five solid crosslinked nanocomposite cylinders and found to be 1.25 g/mL. Based

on these theoretical calculations, 83.9, 87.4, 90.8, and 94.0 wt% NaCl is needed to achieve 75, 80, 85, and 90 vol% porous scaffolds. For example, a formulation of 1 g nanocomposite mixed with 15.62 g NaCl would yield a 90 vol% scaffold.

Scanning Electron Microscopy (SEM)

SEM was applied to examine the pore structure of a scaffold, such as pore size, morphology, and interconnectivity. Cross-sections of cut disc samples were sputter-coated with gold for 2 min at 100 mA using a CrC-150 Sputtering System (Torr International, New Windsor, NY) and observed under a FEI Quanta 400 field emission scanning electron microscope (FEI Company, Hillsboro, OR) at an accelerating voltage of 15 kV.

Microcomputed Tomography (MicroCT)

MicroCT was used to nondestructively and quantitatively measure the three-dimensional porosity and porous interconnectivity of scaffolds. Three 4 × 8 mm cylindrical samples from each scaffold type (n = 3) were scanned with a SkyScan 1172 microCT imaging system (Aartselaar, Belgium) at 10 μm resolution using a voltage of 40 kV, and a current of 250 μA. Image reconstruction and analysis were conducted using the software package provided by SkyScan. The raw images of scaffolds were first reconstructed to serial coronal-oriented tomograms using a 3D cone beam reconstruction algorithm. A thresholding analysis was then performed to determine the threshold value for which grayscale tomograms of scaffolds were most accurately represented by their binarized counterparts in terms of porosity. An optimal threshold value of 40 was applied for all three-dimensional reconstructions and quantitative analysis in this study.

Representative 3D reconstructions (top and 15° angled side views at a camera viewing angle of 10 degree) of porous scaffolds were generated based on the binarized tomograms to visually show the 3D models of scaffold structures. A cylindrical volume of interest (VOI) with a diameter of 3 mm and a height of 6 mm was selected in the center of a scaffold to eliminate potential edge effects. Scaffold porosity was then calculated as:

$$\text{Porosity} = 100\% - \text{vol\% of binarized object (scaffold materials) in VOI.} \tag{3}$$

In this study, interconnectivity was quantified as the fraction of the pore volume in a scaffold that was accessible from the outside through openings of a certain minimum size [19]. A shrink-wrap process was performed between two 3D measurements to shrink the outside boundary of the VOI in a scaffold through any openings whose size is equal to or larger than a threshold value (20–200 μm were used in this study). Interconnectivity was calculated as follows:

$$\text{Interconnectivity} = \left(V - V_{\text{shrink-wrap}}\right) / \left(V - V_m\right) \times 100\% \tag{4}$$

Where V is the total volume of the VOI, $V_{shrink\text{-}wrap}$ is the VOI volume after shrink-wrap processing, and V_m is the volume of scaffold material.

Mercury Intrusion Porosimetry

After microCT scanning, the same scaffold samples were measured for their porosities and pore sizes using an Autoscan-500 mercury intrusion porosimeter (Quantachrome, Boynton Beach, FL). A sample was weighed and placed into the sample chamber, which was evacuated and filled with mercury until an initial pressure of ~ 0.6 psi. The chamber pressure was then increased at a rate of 0.01 psi/second to 50 psi while the intruded volume

of mercury was recorded. The intruded mercury volume per gram sample was measured by the porosimeter and was assumed to be equal to the pore volume (V_{pore}). The porosity (ε) was then calculated as:

$$\varepsilon = \frac{V_{pore}}{V_{pore} + \frac{1}{\rho}} \times 100\% \quad (5)$$

The density of PPF or nanocomposites (ρ) was calculated by measuring the mass and volume of a solid crosslinked cylindrical sample and found to be 1.25 g/mL. The porosimeter also measured the pore size according to the Washburn equation:

$$D = 4\gamma \frac{|\cos\theta|}{P} \quad (6)$$

Where D is the pore diameter, γ is the surface tension of mercury, θ is the contact angle between mercury and the scaffold material (140° as reported in the literature [20]), and P is the pressure.

Compressive Mechanical Testing

Compressive mechanical testing of the 4 × 8 mm cylindrical samples was conducted at room temperature using a uniaxial materials testing machine (Instron Model 5565, Canton, MA) with a 50 N load cell in accordance with the American Society of Testing Materials (ASTM) Standard D695-02a. Scaffold samples were compressed along their long axis at a cross-head speed of 1 mm/min until failure. When a porous scaffold did not fracture, the experiment was halted at 0.5 mm/mm strain. The force and displacement were recorded throughout the compression and converted to stress and strain based on the initial specimen dimensions. The compressive modulus was calculated as the slope of the initial linear portion of the stress-strain curve. The offset compressive yield strength was determined as the stress at which the stress-strain curve intersected with a line drawn parallel to the slope defining the modulus, beginning at 1.0 % strain (offset). The compressive strength was defined as the maximum stress carried by the specimen during the compression testing. Five specimens were tested for each scaffold type (n = 5).

Isolation, Culture, and Storage of Marrow Stromal Cells (MSCs)

Rat bone MSCs were harvested and cultured based on established protocols [21, 22]. Briefly, 6–8 week old male Wistar rats (Charles River Laboratories, Wilmington, MA) were anesthetized using 4% isofluorane in oxygen and then euthanized by inhalation of CO_2. Under aseptic conditions, the femora and tibiae were excised from the hind limbs and the external soft tissue was discarded. The proximal ends of the femora and the distal ends of the tibiae were cut off. An 18-gauge needle was inserted into the diaphyses through the knee joint end of each bone, and the marrow was flushed out with 5 mL complete osteogenic media containing α-Eagle minimum essential media (α-MEM, Sigma-Aldrich, St. Louis, MO), 10 vol% fetal bovine serum (FBS, BioWhittaker, Walkersville, MD), 50 μg/mL gentamicin, 100 μg/mL ampicillin, 0.5 μg/mL fungizone, 50 μg/mL. L-ascorbic acid, 0.01 M β-glycerophosphate, and 10^{-8} M dexamethasone (all from Sigma-Aldrich). The resulting marrow pellets were broken up by trituration, and the cell suspensions from all bone marrows were combined and plated in 75-cm^2 tissue culture flasks for 6 days under standard cell-culture conditions, i.e. 37°C, 95% relative humidity, and 5% CO_2 / 95% air environment. The osteogenic media were changed at 1 and 3 days to remove the nonadherent cell population. At the end of this primary culture, MSCs were enzymatically

lifted from the flasks with 2 mL of a concentrated trypsin solution (0.25% trypsin / 0.02% ethylenediaminetetraacetic acid), centrifuged at 400 g for 10 min, and resuspended at a concentration of 3 million cells / mL FBS with 10 vol% dimethyl sulfoxide (DMSO, Sigma-Aldrich). This cell suspension was aliquoted in 1.5 mL cryovials, put into a cryogenic freezing container, kept at −80 °C overnight, and then transferred to a liquid nitrogen storage tank until use.

MSC Culture on Porous Scaffolds

MSCs were thawed, suspended in media, pelleted, and resuspended in a known amount of osteogenic media to remove DMSO. The cell suspensions were cultured in 75-cm^2 tissue culture flasks at a density of one million cells per flask for 7 days with complete osteogenic media changed at 1, 3, and 5 days. Prior to cell seeding, 6.5 × 2 mm disc scaffolds were sterilized and prewetted based on an established process [23]. Briefly, scaffolds were first sterilized with ethylene oxide gas for 14 h. Twelve samples from each scaffold group were then prewetted with a gradient ethanol series from 100 % to 70 % by centrifugation, rinsed with phosphate buffered saline (PBS) three times and then with osteogenic media twice and left in a incubator overnight. Afterwards, the passaged MSCs were lifted, resuspended in osteogenic media, and seeded on the prepared scaffolds at a density of 250,000 cells/scaffold in 25 μL media. Cells were allowed to attach for 3 h before adding 1 mL complete media to each well of the 24-well plates. At 1, 3, and 7 days, the media were changed and four scaffolds of each sample group were removed and rinsed with PBS. Three of the four scaffolds were stored in 1.5 mL distilled and deionized water at −20°C for the PicoGreen DNA assay and one scaffold was immediately used for scanning confocal microscopy and then scanning electron microscopy.

Scaffold Cellularity Assays

Scaffold cellularity was quantified using the PicoGreen assay kit from Molecular Probe (Eugene, OR) to measure fluorometric double-stranded DNA (dsDNA) content [22]. The PicoGreen dye binds to the major grooves of dsDNA and the resulting fluorescence intensity linearly corresponds to dsDNA concentration in solution. To extract cellular DNA into the water solution, the stored scaffolds were first subjected to three freeze/thaw cycles (10 min in liquid nitrogen and 10 min in a 37 °C water bath) followed by sonication for 30 min. According to the manufacturer's instructions, working buffer, sample solutions or dsDNA standard solutions (0–6 μg/mL), and PicoGreen dye were sequentially added into each well of a 96-well plate at 100, 50, and 150 μL per well, respectively. After a 10-min incubation period in the dark at room temperature, the fluorescence of each well was measured with a BIOTEK Instruments Flx800 plate reader (Winooski, VT) using an excitation wavelength of 480 nm and an emission wavelength of 520 nm. The cell number on each scaffold was determined by correlating measured DNA amount with a known number of MSCs, which was 3.04 pg DNA per cell in this study.

The cellularity on the porous scaffolds was also visualized by both confocal microscopy and SEM. A scaffold from each sample group was first stained with 1 mL LIVE/DEAD reagent (2 μM calcein AM and 4 μM ethidium homodimer-1 (EthD-1), Molecular Probes, Eugene, OR) and then imaged with a laser scanning confocal microscope (Zeiss LSM 510 Axiovert, Carl Zeiss, Germany) under an Argon laser excited at 488 nm with emitted light collected at 515 nm for calcein AM (live cells) and 635 nm for EthD-1 (dead cells). The cytoplasm of live cells was stained with the calcein green dye and the cell nucleus of dead cells was stained with the EthD-1 red dye. The same samples were subsequently immersed in 2.5 % glutaraldehyde to fix the cells, dehydrated in a gradient series of ethanol, air-dried, and then vacuum-dried overnight. Finally, the scaffold surface was sputter-coated with gold and observed with a FEI Quanta 400 field emission SEM at an accelerating voltage of 15 kV.

Statistical Analysis

All statistical comparisons were conducted with a 95% confidence interval ($p < 0.05$). Single-factor analysis of variance (ANOVA) was conducted to identify significant differences among treatment groups. When significant differences were present, Tukey's Honestly Significantly Different (HSD) multiple-comparison test was used to determine the potential effects. The experimental data were expressed as means ± standard deviation.

RESULTS

Porous scaffolds made of PPF, the US-tube nanocomposite, and the F-US-tube nanocomposite were successfully fabricated by the thermal-crosslinking particulate-leaching technique at four NaCl porogen fractions, 75, 80, 85, and 90 vol%. Two different size scaffold samples were produced to meet the requirements of different characterization tests: cylindrical samples (4 mm diameter and 8 mm height) for scaffold characterization by microCT, porosimetry, and compressive mechanical testing; and circular disc samples (6.5 mm diameter and 2 mm thickness) for SEM and three-dimensional culture of rat MSCs.

Scaffold Characterization by SEM

The cross-sections of NaCl-leached scaffolds are shown in the SEM images presented in Figure 2. All scaffolds were highly porous and pores surrounded by thin walls of PPF or nanocomposites appeared well interconnected with each other. Most pores in 75 and 80 vol % scaffolds apparently maintained the cubic shape and size (300–500 μm) of NaCl crystals. Pores became more irregular as NaCl fraction increased with thinner walls and more and larger openings that connected pores inside the scaffolds. There was no characteristic difference among the SEM images of each scaffold made of PPF, US-tube nanocomposite, or F-US-tube nanocomposite at the same NaCl fractions.

Scaffold Characterization by MicroCT

Representative 3D images of porous F-US-tube nanocomposite scaffolds reconstructed by microCT are presented in Figure 3A. Top views of each scaffold revealed structures very similar to those seen in SEM images. That is, more pores were surrounded by thinner walls with larger interconnects as NaCl fraction increased from 75 to 90 vol%. These observations were consistent by going through all individual cross-sections of the microCT reconstructed images without physical sectioning. In addition, representative 3D models of scaffolds can be examined from any angle of view at up to 10 μm resolution by shifting, rotating, and magnifying them in virtual space. For example, the 3D images of side view provided further visual support of increasing scaffold porosity with increasing porogen content. Representative 3D models of PPF scaffolds and the US-tube nanocomposite scaffolds appeared similar to Figure 3A (data not shown).

The porosity of each scaffold with 75–90 vol% NaCl content was determined from microCT data (Figure 3B and Table 1). The measured porosity values of NaCl-leached scaffolds closely matched the theoretical porosities of 75, 80, 85, and 90 vol% scaffolds. Moreover, there was no significant difference in microCT-measured porosity among scaffolds made of PPF, US-tube and F-US-tube nanocomposites.

Figure 3C shows the results of interconnectivity analysis of F-US-tube nanocomposite scaffolds with various NaCl fractions. As an opening between two pores can be called an interconnection only when it is larger than a certain size, the value of interconnectivity is highly dependent on the defined minimum sizes. From the computed data, more than 99% of the pores inside 75–90 vol% scaffolds were connected to their outside environment through openings of at least 20 μm. However, the interconnectivity of 75 vol% scaffolds dropped

from 98.6 ± 0.1 % for 40 μm minimum connection size to mere 30.0 ± 5.1 % for 200 μm. Interconnectivity of 80, 85, and 90 vol% scaffolds followed the same trend. At each minimum connection size, interconnectivity declined with decreasing porosity from 90 to 75 vol% and the difference among different porous scaffolds became significant as the minimum connection size increased. Scaffolds of PPF and US-tube nanocomposite showed similar trends in interconnectivity vs. 75–90 vol% NaCl content (Table 2).

Scaffold Characterization by Porosimetry

Scaffold porosity was also determined through the use of mercury intrusion porosimetry as presented in Figure 4A. The porosity values measured by porosimetry were comparable with those calculated by microCT for all scaffolds regardless of material or porosity (Table 1). There was no significant difference in porosity among scaffold material groups of PPF, US-tube nanocomposite, and F-US-tube nanocomposite at the same porogen fractions. While 80, 85, and 90 vol% scaffolds all had mean pore sizes ranging from 80 to 100 μm, the mean pore sizes of 75 vol% scaffolds were only 40–50μm (Figure 4B). No significant difference in mean pore size of scaffold was detected among different material groups at the same porogen content. These data further confirmed that porous scaffolds were fabricated with controllable porosities of 75–90 vol% from PPF and nanocomposite materials via the NaCl-leaching technique.

Compressive Mechanical Properties

Compressive mechanical properties of porous scaffolds are shown as compressive modulus, offset yield strength, and compressive strength in Figure 5. Compressive mechanical properties of each type of scaffold significantly decreased as the porogen fraction increased from 75 vol% to 90 vol%. For example, the compressive moduli of PPF scaffolds were 7.5 ± 3.1, 3.5 ± 0.9, 0.48 ± 0.22, and 0.058 ± 0.016 MPa at NaCl contents of 75, 80, 85, and 90 vol %, respectively, which is more than a 100-fold decline in compressive modulus as scaffolds changed from 75 vol% to 90 vol%. As the standard deviations were large for each sample group, only a few significant differences were detected among the three types of materials: scaffolds made of F-US-tube nanocomposite were significantly stronger than PPF scaffolds at both 80 and 85 vol% porogen fractions in terms of offset yield strength and compressive strength, and the offset yield strength of F-US-tube nanocomposite scaffolds was also significantly higher than that of US-tube nanocomposite scaffolds at 85 vol% NaCl content.

MSC Cellularity on Porous Scaffolds

The number of cells in each MSC/scaffold construct after 1, 3, and 7 days in culture is shown in Figure 6. All scaffolds considered in this study (three different types of materials with four different porosities) supported the adhesion and proliferation of the seeded rat MSCs over the seven day *in vitro* culture period. Of the 250,000 seeded cells, approximately 110,000–140,000 MSCs attached to each scaffold after 1 day in culture. The cell number on each scaffold increased over time, reaching approximately 180,000–210,000 cells/scaffold. No significant difference in cell number was detected either among three different materials for any NaCl fraction or among four different NaCl fractions for any material.

MSC attachment and proliferation on different types of scaffolds with various porosities were also visualized with confocal microscopy. Stained with calcein AM, the live cells emitted green fluorescence under the confocal microscope. As seen in Figure 7 A1–4, viable MSCs covered the struts/walls of the nanocomposite of 75–90 vol% scaffolds after 1 day in culture. Then, the MSCs started spreading over the scaffold surface and growing into the open pores on day 3 (Figure 7 B1–4). After 7 days, highly distributed MSCs and their extracellular matrix filled/covered most of the pores on the surface of scaffolds (Figure 7 C1–4).

SEM images of the same MSC/scaffold constructs after confocal microscopy further support the observation of MSC adhesion and proliferation on all scaffolds in this study. After seeding, attached MSCs appeared in round shapes (Figure 8 A1–4). However, on day 3, MSCs spread out and firmly attached to the scaffolds with some pores partially covered by growing cells (Figure 8 B1–4). On day 7, most pores were totally covered by MSCs and matrix, resulting in a flat appearance of the originally porous surface (Figure 8 C1–4). It was difficult to distinguish embedded MSCs from their surrounding matrix.

DISCUSSION

Previous studies in our laboratory demonstrated that single-walled carbon nanotubes, and particularly US-tubes, can be applied as reinforcing agents to significantly enhance the mechanical properties of crosslinked PPF polymer [4–6]. Moreover, Zanello et al. showed excellent osteoblast proliferation on carbon nanotube substrates [24]. These discoveries suggest that carbon nanotube nanocomposites hold great promise as scaffold materials for bone tissue engineering applications.

There were three objectives in this study: (1) to develop highly porous scaffolds from PPF, US-tube nanocomposite, and F-US-tube nanocomposite using a particulate-leaching technique; (2) to evaluate the pore structures and compressive mechanical properties of these scaffolds; and (3) to investigate their *in vitro* osteoconductivity. Osteoconductivity here refers to a scaffold's ability to serve as a substrate for bone cell adhesion and proliferation [2]. Porosity in a range of 75 to 90 vol% and different nanocomposites were examined for their effects on scaffold fabrication, scaffold structure, compressive mechanical properties, and MSC adhesion and proliferation.

Scaffold Fabrication

Tissue engineering scaffolds for trabecular bone regeneration may mimic the corresponding bone morphology with porosities varying from 50–90% [3]. Such high porosities are critical for a regenerative process as they may provide large surface area for cell adhesion and proliferation and allow for vascularized tissue ingrowth. There are various methods to generate highly porous scaffolds for tissue engineering, including solvent casting/particulate leaching, gas forming, fiber bonding, electrospinning, rapid prototyping, phase separation, and emulsion templating [24–31]. As a convenient, reliable, and economical technique, NaCl-leaching is widely used for scaffold fabrication. The NaCl crystals used in this study were in the size range of 300–500 μm in order to generate optimum-size pores for osteogenesis [3, 9]. Since the PPF polymer and the nanocomposites are injectable and crosslinkable, this thermal-crosslinking NaCl-leaching technique also avoids using any organic solvent like many other methods. In addition, stable PPF and its composite scaffolds with porosity as high as 90 vol% were created for the first time using this technique [11, 32]. Scaffolds with 95 vol% porosity were also produced but were too brittle to be handled for characterization.

Characterization of Pore Structures

Porosity, pore size, and pore interconnectivity are important parameters for bone tissue engineering scaffolds that influence osteoblast migration and bone tissue ingrowth. For example, only pores with diameter greater than 10 μm may allow for bone cell migration. Further, pore diameters of 300–400 μm were reported to be optimal for hydroxyapatite scaffolds in terms of new bone formation and vascularization [3]. Moreover, high pore interconnectivity is a scaffold requirement needed not only to facilitate exchange of nutrients and metabolic wastes but also to enable tissue ingrowth and vascularization. To characterize the morphological features of pores within scaffolds, SEM, mercury intrusion

porosimetry and microCT are commonly used [33]. SEM allows direct imaging of pore structures in high resolutions to qualitatively evaluate porosity, pore size, and interconnectivity. However, quantitative measurements are difficult to perform from 2D SEM images and samples can not be reused due to sectioning and coating during sample preparation. Mercury intrusion porosimetry, also a destructive technique, can accurately determine porosity and pore size. Open pores as small as 2.13 μm diameter can be intruded with mercury at pressures up to 50 psi. On the contrary, microCT can not only nondestructively quantify porosity and interconnectivity, but also offer 3D visualization of scaffold morphology from any angle of view at a high spatial resolution. Beam hardening and thresholding difficulty are the main drawbacks of this computational technique [33]. Therefore, we used these three complementary methods together to characterize the architecture of our scaffolds.

There was no significant difference in porosity, pore size, and pore interconnectivity among scaffolds made of the three different materials. Porosities of all NaCl-leached scaffolds were precisely tuned to the designed 75, 80, 85, and 90 vol% by adding proper amounts of NaCl. This was supported by both microCT and porosimetry measurements (Table 1). PPF scaffolds with 75 vol% porosity contained pore networks connecting scaffold interiors to surface openings [19, 34] as observed from the SEM and microCT images of this study (Figure 2 and 3). When porosity further increased, the walls surrounding the pores appeared thinner and the connections became larger. This observation of enhanced pore interconnectivity with larger connection sizes for higher porosities was supported by microCT calculations (Table 2). Since the pores were nearly 100% interconnected through connections of 20 μm or larger for all scaffolds in this study, it was not surprising to see that the porosities measured by microCT or porosimetry matched well with each other, although microCT determined porosity based on all pores while porosimetry only measured interconnected pores. In addition, the higher fractions of small connections (~ 20% connections < 100 μm) in 75 vol% scaffolds may explain their significantly smaller mean pore sizes compared to 80–90 vol% scaffolds (Figure 4B). Due to random porogen distribution in PPF or nanocomposites and their interactions during thermal-crosslinking, salt leaching, and drying, NaCl-leached scaffolds possessed irregular pore architectures, which may cause large variations in mechanical properties for different samples of the same material and porosity group.

Compressive Mechanical Properties

F-US-tubes were covalently wrapped with 40 wt% dodecyl groups (Figure 1), which further improved the dispersion of carbon nanotubes in PPF polymer. Our previous study showed that better dispersed single-walled carbon nanotubes could provide greater mechanical reinforcements [5]. In this study, there was also a general trend of enhancement in compressive mechanical properties of F-US-tube nanocomposite over pure PPF or even US-tube nanocomposite for various scaffolds, although many of the reinforcements were not significant due to the intrinsically large variations in the mechanical properties (Figure 5). It has been established that scaffold porosity plays a major role in determining the compressive mechanical moduli and yield strengths in accordance with power law relationships [7]. These power-law declines in mechanical properties with higher porosity set a tradeoff for the benefit of increasing porosity of scaffolds to improve pore interconnectivity for better tissue ingrowth. For example, although a 90 vol% scaffold may provide enhanced nutrient transport for seeded cells [35], such scaffolds made from PPF or the nanocomosites would possess compressive strengths of only 11–15 KPa, which are too weak to be used for replacement of load-bearing bone tissues. Therefore, porosity should be finely controlled to reach a balance between interconnectivity and mechanical properties for scaffolds designed to meet the specific needs of bone repair.

MSC Cellularity on Porous Scaffolds

Since these scaffolds are being developed for bone tissue engineering, MSCs capable of osteogenic differentiation provide an excellent *in vitro* model to further assess their suitability for such applications. Before spreading, MSCs have a diameter of less than 10 μm and thus may be able to migrate into all scaffolds, which were 100% interconnected through 20 μm or larger connections. Due to the diffusive transport limitations of static culture, cells tended to attach and proliferate only on the top layers of the three-dimensional scaffolds in this study (Figure 7 and 8). That may explain the nonsignificant trends of increasing cellularity of MSC/scaffold constructs with increasing porosity although more space was allowed for cell attachment and proliferation (Figure 6). Another limitation for cellularity of seeded MSCs could be the lack of angiogenesis (new blood vessel formation) in our *in vitro* culture systems [9]. Although the present study demonstrated the adhesion and proliferation of seeded cells, additional studies will be needed to evaluate the osteoblastic differentiation of marrow stromal cells. In this study, MSCs were able to grow well on all scaffolds without a significant difference in cellularity among PPF, US-tube nanocomposite, and F-US-tube nanocomposite, indicating that all these materials are osteoconductive *in vitro*.

CONCLUSION

This study demonstrated that scaffolds made of PPF polymer, US-tube nanocomposite, and F-US-tube nanocomposite can be fabricated at precisely controllable porosities of 75, 80, 85, and 90 vol% by a thermal-crosslinking particulate-leaching technique. Pore structures of these highly porous scaffolds were characterized with SEM, microCT, and mercury intrusion porosimetry. No matter which material was used, all scaffolds were created with specific porosities and nearly 100% interconnectivity through connections of at least 20 μm. The pore connections became larger as scaffold porosity increased, which may explain the significant increase in mean pore size of 80–90 vol% scaffolds compared to 75 vol% scaffolds. However, higher porosity significantly decreased the compressive mechanical properties of the scaffolds, compromising the advantages of high porosity. F-US-tube nanocomposites reinforced the scaffolds although some mechanical enhancements were not significant due to sample variations. Finally, the osteoconductivity of all these scaffolds was supported by the excellent attachment and proliferation of MSCs under static culture conditions. Therefore, F-US-tube nanocomposites can be fabricated into equally porous scaffolds for MSC culture but with mechanical properties higher than or similar to those of pure PPF and US-tube nanocomposites. Such highly porous F-US-tube nanocomposite scaffolds with controllable pore structures and mechanical properties demonstrate a promising development in bone tissue engineering scaffolds.

Acknowledgments

This research was supported by grants from the National Institutes of Health (R01 AR42639 and R01 DE15164), the Nanoscale Science and Engineering Initiative of the National Science Foundation (EEC-0118001), the National Science Foundation (DMR 9875321), and the Robert A. Welch Foundation. The work of W.E.B. was sponsored by Welch (C-0490) and NSF (CHE-0450085) grants. We thank Dr. Simon Young for assistance with the microcomputed tomography and Prof. Kyriacos A. Athanasiou and Gwen Hoben for help with the compressive mechanical testing.

References

1. Langer R, Vacanti JP. Tissue Engineering. Science. 1993; 260(5110):920–26. [PubMed: 8493529]
2. Mistry AS, Mikos AG. Tissue engineering strategies for bone regeneration. Adv Biochem Eng Biotechnol. 2005; 94:1–22. [PubMed: 15915866]
3. Karageorgiou V, Kaplan D. Porosity of 3D biornaterial scaffolds and osteogenesis. Biomaterials. 2005; 26(27):5474–91. [PubMed: 15860204]

4. Shi X, Hudson JL, Spicer PP, Tour JM, Krishnamoorti R, Mikos AG. Rheological behaviour and mechanical characterization of injectable poly(propylene fumarate)/single-walled carbon nanotube composites for bone tissue engineering. Nanotechnology. 2005; 16(7):S531–S38. [PubMed: 21727474]
5. Shi X, Hudson JL, Spicer PP, Tour JM, Krishnamoorti R, Mikos AG. Injectable nanocomposites of single-walled carbon nanotubes and biodegradable polymers for bone tissue engineering. Biomacromolecules. 2006; 7(7):2237–42. [PubMed: 16827593]
6. Sitharaman B, Shi X, Tran LA, Spicer PP, Rusakova I, Wilson LJ, et al. Injectable in situ crosslinkable nanocomposites of biodegradable polymers and carbon nanostructures for bone tissue engineering. J Biomater Sci Polym Ed. 2007 in press.
7. Thomson RC, Yaszemski MJ, Powers JM, Mikos AG. Fabrication of biodegradable polymer scaffolds to engineer trabecular bone. J Biomater Sci Polym Ed. 1995; 7(1):23–38. [PubMed: 7662615]
8. Harrison BS, Atala A. Carbon nanotube applications for tissue engineering. Biomaterials. 2007; 28(2):344–53. [PubMed: 16934866]
9. Ishaug SL, Crane GM, Miller MJ, Yasko AW, Yaszemski MJ, Mikos AG. Bone formation by three-dimensional stromal osteoblast culture in biodegradable polymer scaffolds. J Biomed Mater Res. 1997; 36(1):17–28. [PubMed: 9212385]
10. Ishaug-Riley SL, Crane-Kruger GM, Yaszemski MJ, Mikos AG. Three-dimensional culture of rat calvarial osteoblasts in porous biodegradable polymers. Biomaterials. 1998; 19(15):1405–12. [PubMed: 9758040]
11. Fisher JP, Holland TA, Dean D, Engel PS, Mikos AG. Synthesis and properties of photocross-linked poly(propylene fumarate) scaffolds. J Biomater Sci Polym Ed. 2001; 12(6):673–87. [PubMed: 11556743]
12. Shung AK, Timmer MD, Jo S, Engel PS, Mikos AG. Kinetics of poly(propylene fumarate) synthesis by step polymerization of diethyl fumarate and propylene glycol using zinc chloride as a catalyst. J Biomater Sci Polym Ed. 2002; 13(1):95–108. [PubMed: 12003078]
13. Timmer MD, Ambrose CG, Mikos AG. Evaluation of thermal- and photo-crosslinked biodegradable poly(propylene fumarate)-based networks. J Biomed Mater Res A. 2003; 66A(4): 811–18. [PubMed: 12926033]
14. Gu Z, Peng H, Hauge RH, Smalley RE, Margrave JL. Cutting single-wall carbon nanotubes through fluorination. Nano Lett. 2002; 2(9):1009–13.
15. Chiang IW, Brinson BE, Huang AY, Willis PA, Bronikowski MJ, Margrave JL, et al. Purification and characterization of single-wall carbon nanotubes (SWNTs) obtained from the gas-phase decomposition of CO (HiPco process). J Phys Chem B. 2001; 105(35):8297–301.
16. Liang F, Alemany LB, Beach JM, Billups WE. Structure analyses of dodecylated single-walled carbon nanotubes. J Am Chem Soc. 2005; 127(40):13941–48. [PubMed: 16201816]
17. Liang F, Sadana AK, Peera A, Chattopadhyay J, Gu ZN, Hauge RH, et al. A convenient route to functionalized carbon nanotubes. Nano Lett. 2004; 4(7):1257–60.
18. Timmer MD, Carter C, Ambrose CG, Mikos AG. Fabrication of poly(propylene fumarate)-based orthopaedic implants by photo-crosslinking through transparent silicone molds. Biomaterials. 2003; 24(25):4707–14. [PubMed: 12951014]
19. Moore MJ, Jabbari E, Ritman EL, Lu LC, Currier BL, Windebank AJ, et al. Quantitative analysis of interconnectivity of porous biodegradable scaffolds with microcomputed tomography. J Biomed Mater Res A. 2004; 71A(2):258–67. [PubMed: 15376269]
20. Lowell, S.; Shields, JE.; Thomas, MA.; Thommes, M. Characterization of porous solids and powders : surface area, pore size, and density. 4th ed.. Kluwer Academic Publishers; Boston, MA: 2005.
21. Holtorf HL, Jansen JA, Mikos AG. Flow perfusion culture induces the osteoblastic differentiation of marrow stromal cell-scaffold constructs in the absence of dexamethasone. J Biomed Mater Res A. 2005; 72A(3):326–34. [PubMed: 15657936]
22. Datta N, Holtorf HL, Sikavitsas VI, Jansen JA, Mikos AG. Effect of bone extracellular matrix synthesized in vitro on the osteoblastic differentiation of marrow stromal cells. Biomaterials. 2005; 26(9):971–77. [PubMed: 15369685]

23. Pham QP, Sharma U, Mikos AG. Electrospun poly(epsilon-caprolactone) microfiber and multilayer nanofiber/microfiber scaffolds: Characterization of scaffolds and measurement of cellular infiltration. Biomacromolecules. 2006; 7(10):2796–805. [PubMed: 17025355]
24. Zanello LP, Zhao B, Hu H, Haddon RC. Bone cell proliferation on carbon nanotubes. Nano Lett. 2006; 6(3):562–67. [PubMed: 16522063]
25. Mikos AG, Bao Y, Cima LG, Ingber DE, Vacanti JP, Langer R. Preparation of poly(glycolic acid) bonded fiber structures for cell attachment and transplantation. J Biomed Mater Res. 1993; 27(2): 183–9. [PubMed: 8382203]
26. Mikos AG, Sarakinos G, Leite SM, Vacanti JP, Langer R. Laminated three-dimensional biodegradable foams for use in tissue engineering. Biomaterials. 1993; 14(5):323–30. [PubMed: 8507774]
27. Mikos AG, Thorsen AJ, Czerwonka LA, Bao Y, Langer R, Winslow DN, et al. Preparation and characterization of poly(L-lactic acid) foams. Polymer. 1994; 35(5):1068–77.
28. Mooney DJ, Baldwin DF, Suh NP, Vacanti LP, Langer R. Novel approach to fabricate porous sponges of poly(D,L-lactic-co-glycolic acid) without the use of organic solvents. Biomaterials. 1996; 17(14):1417–22. [PubMed: 8830969]
29. Lo H, Ponticiello MS, Leong KW. Fabrication of controlled release biodegradable foams by phase separation. Tissue Eng. 1995; 1(1):15–28. [PubMed: 19877912]
30. Pham QP, Sharma U, Mikos AG. Electrospinning of polymeric nanofibers for tissue engineering applications: A review. Tissue Eng. 2006; 12(5):1197–211. [PubMed: 16771634]
31. Whang K, Thomas CH, Healy KE, Nuber G. A novel method to fabricate bioabsorbable scaffolds. Polymer. 1995; 36(4):837–42.
32. Cooke MN, Fisher JP, Dean D, Rimnac C, Mikos AG. Use of stereolithography to manufacture critical-sized 3D biodegradable scaffolds for bone ingrowth. J Biomed Mater Res B. 2003; 64B(2): 65–69.
33. Rajagopalan S, Lu LC, Yaszemski MJ, Robb RA. Optimal segmentation of microcomputed tomographic images of porous tissue-engineering scaffolds. J Biomed Mater Res A. 2005; 75A(4): 877–87. [PubMed: 16142796]
34. Ho ST, Hutmacher DW. A comparison of micro CT with other techniques used in the characterization of scaffolds. Biomaterials. 2006; 27(8):1362–76. [PubMed: 16174523]
35. Fisher JP, Vehof JW, Dean D, van der Waerden JP, Holland TA, Mikos AG, et al. Soft and hard tissue response to photocrosslinked poly(propylene fumarate) scaffolds in a rabbit model. J Biomed Mater Res A. 2002; 59A(3):547–56.
36. Freed LE, Vunjaknovakovic G, Biron RJ, Eagles DB, Lesnoy DC, Barlow SK, et al. Biodegradable polymer scaffolds for tissue engineering. Bio-Technology. 1994; 12(7):689–93. [PubMed: 7764913]

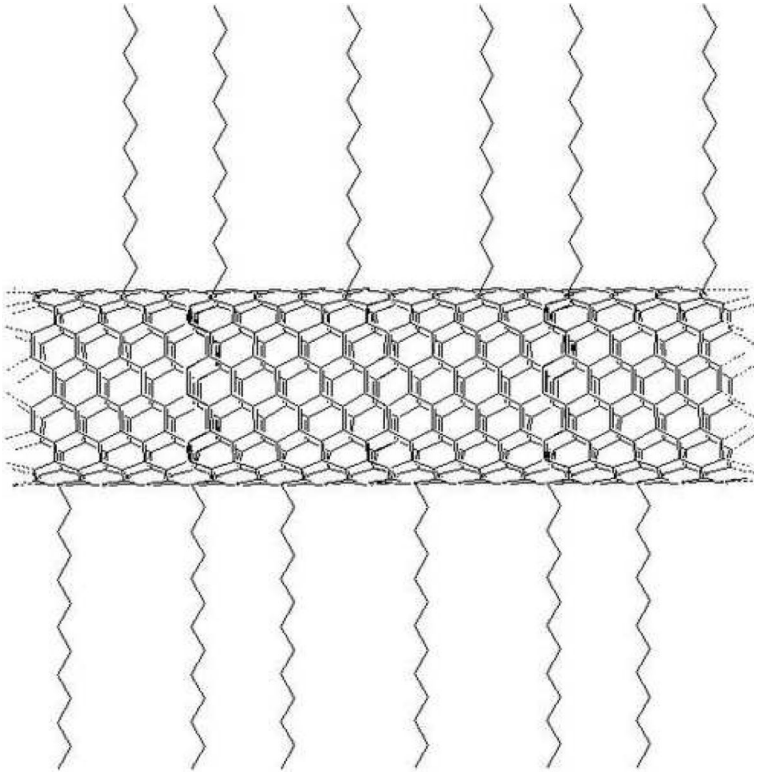

Figure 1.
Depiction of a functionalized ultra-short single-walled carbon nanotube (F-US-tube) with dodecyl groups attached to its sidewall.

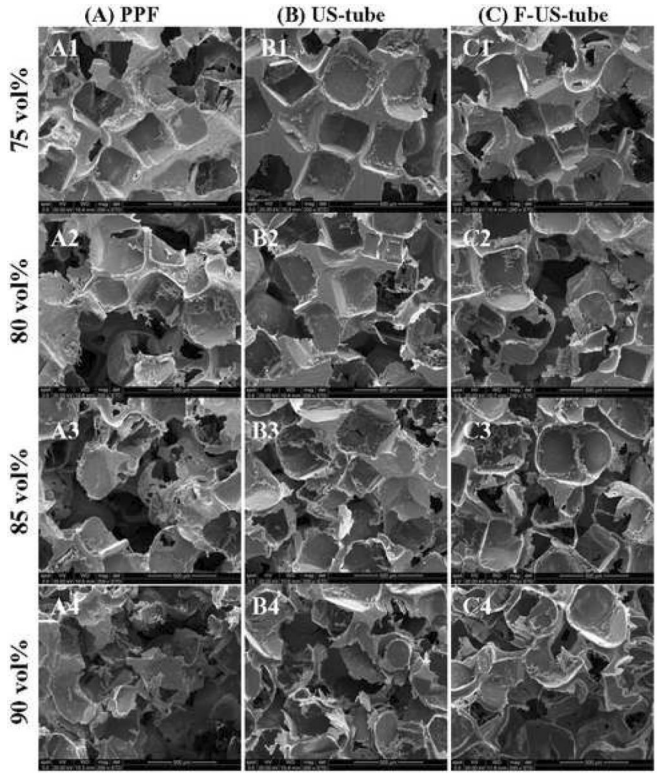

Figure 2.
SEM images of scaffolds made of (A1–4) PPF, (B1–4) US-tube nanocomposite, and (C1–4) F-US-tube nanocomposite with increasing porogen fractions of 75, 80, 85, 90 vol% (from top to bottom). Scale bar represents 500 μm.

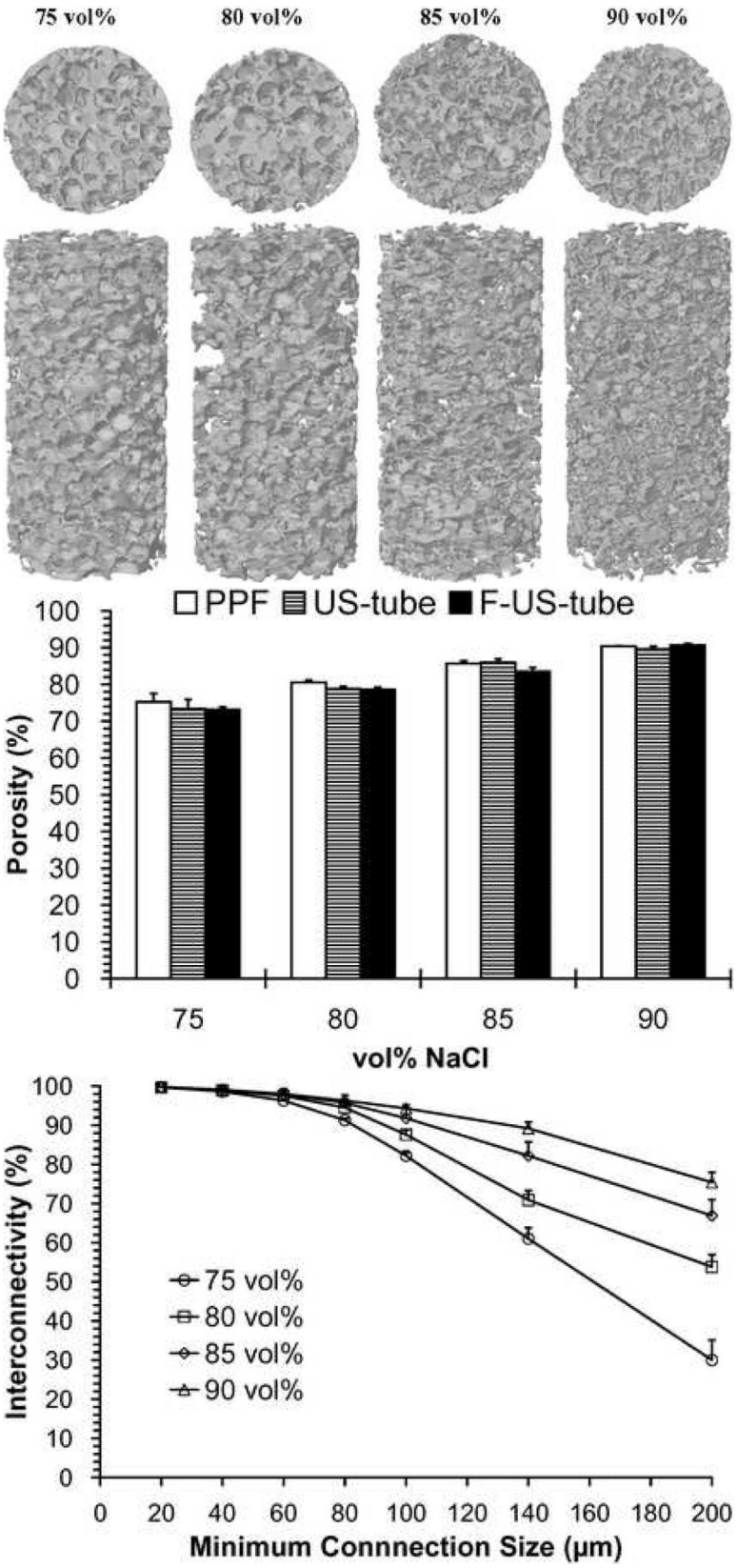

Figure 3.

Results of microCT analysis: (A) representative 3D reconstructions (top and 15° angled side views) of F-US-tube nanocomposite scaffolds with various NaCl fractions; (B) porosity of different scaffolds with 75–90 vol% porogen contents as determined by microCT; there was significant difference among different vol% NaCl groups for each type of material, but no significant difference among different material groups for each porogen content; (C) interconnectivity vs. minimum connection size for F-US-tube nanocomposite scaffolds with various NaCl fractions. Error bars represent standard deviations; n = 3.

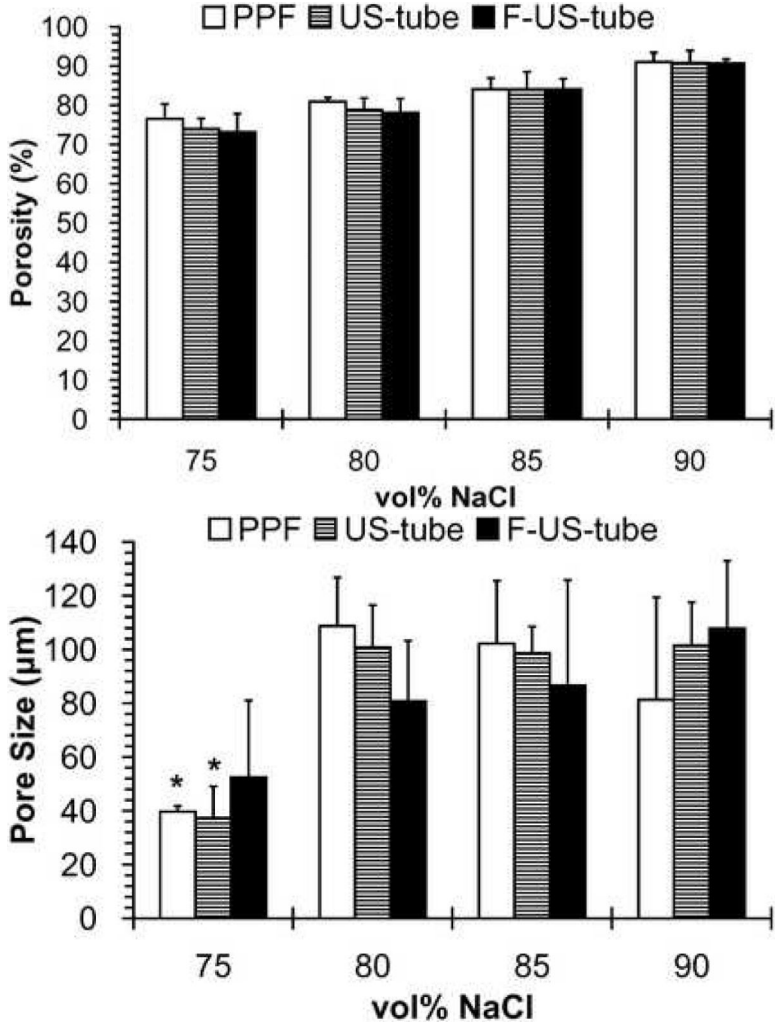

Figure 4.

(A) Porosity and (B) pore size of different scaffolds with 75–90 vol% porogen contents as determined by mercury intrusion porosimetry. Error bars represent standard deviations; n = 3. The symbol "*" indicates a statistically significant difference between 75 vol% scaffolds and other vol% scaffolds ($p < 0.05$).

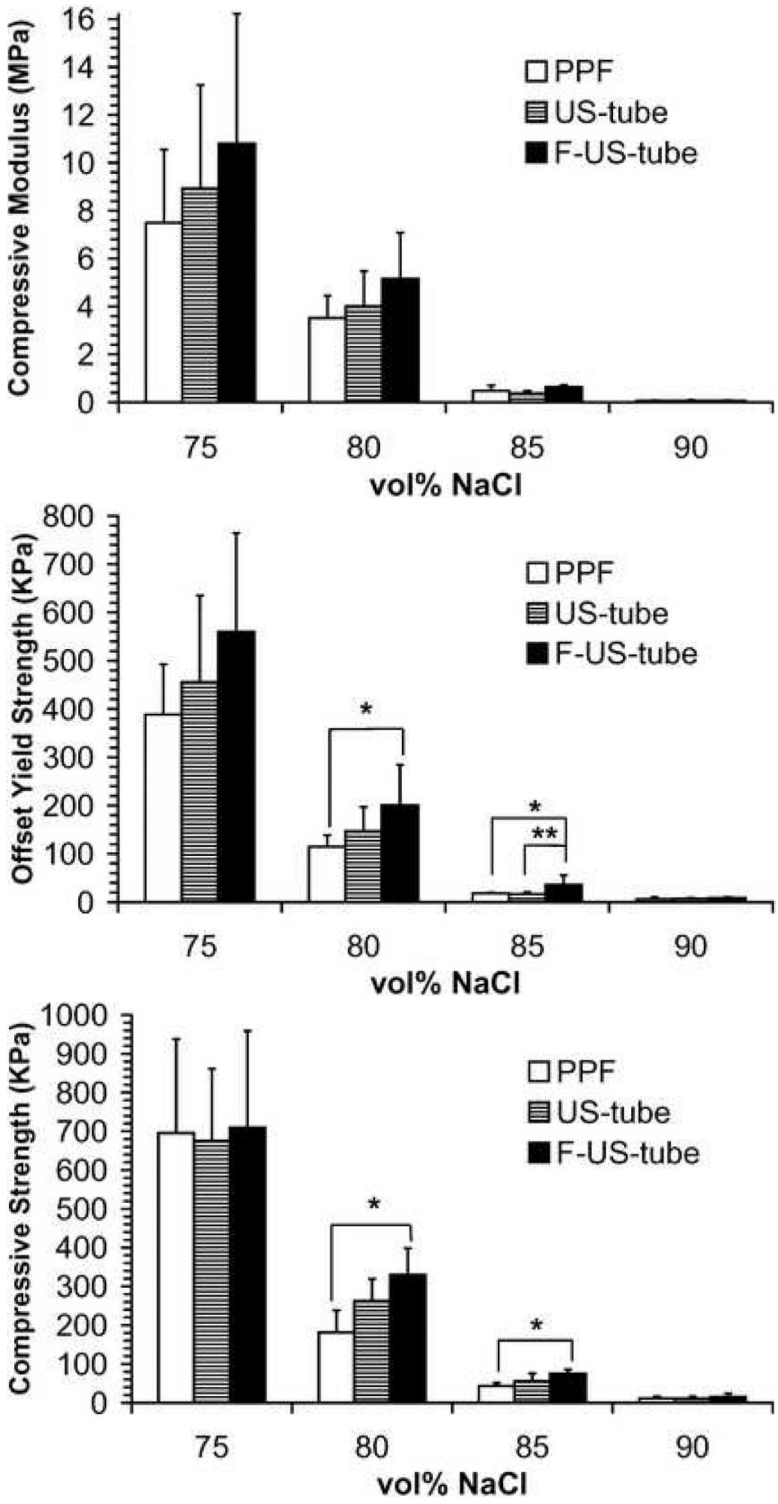

Figure 5.

Compressive mechanical properties of porous scaffolds made of different materials as a function of porogen fraction: (A) compressive modulus, (B) offset yield strength, and (C) compressive strength. Error bars represent standard deviations; n = 5. The symbol "*" indicates a statistically significant difference between two scaffold groups ($p < 0.05$).

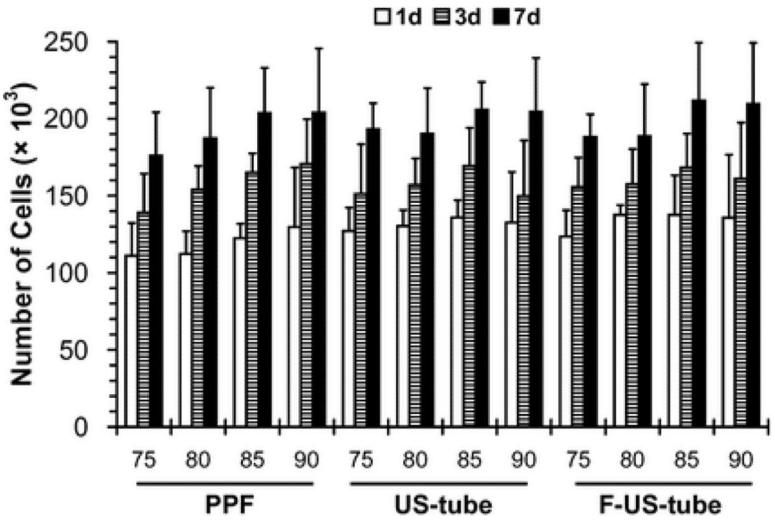

Figure 6.

Cellularity of MSCs cultured on porous scaffolds made of PPF, US-tube nanocomposite, and F-US-tube nanocomposite with 75, 80, 85, and 90 vol% NaCl fractions for 1, 3, and 7 days. Error bars represent standard deviations; n = 3.

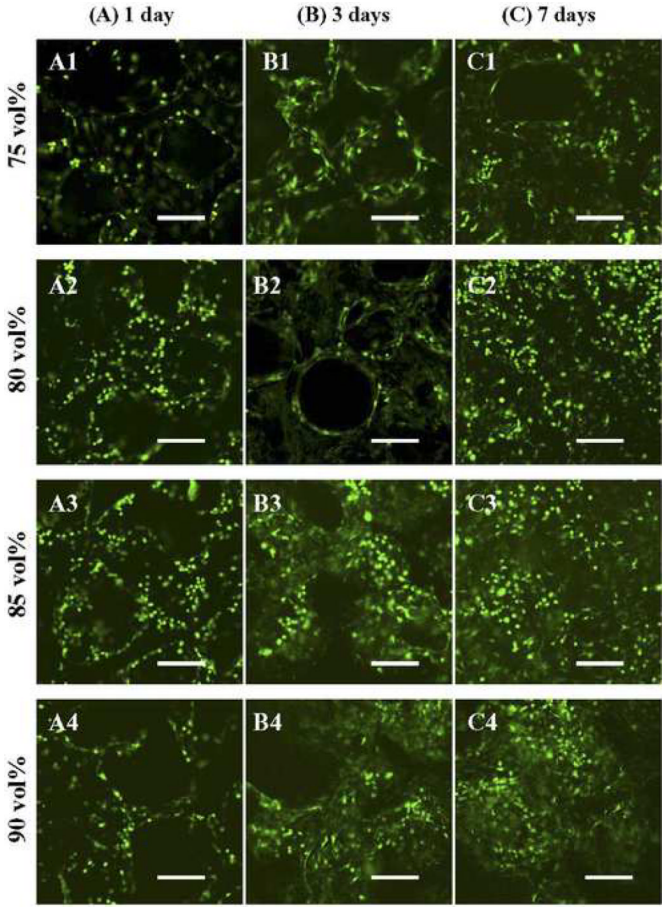

Figure 7.

Confocal microscopy images of F-US-tube nanocomposite scaffolds with porogen fractions of 75, 80, 85, 90 vol % (from top to bottom) after seeding MSCs for (A1–4) 1 day, (B1–4) 3 days, and (C1–4) 7 days, all treated with LIVE/DEAD reagent. Scale bar represents 200 μm.

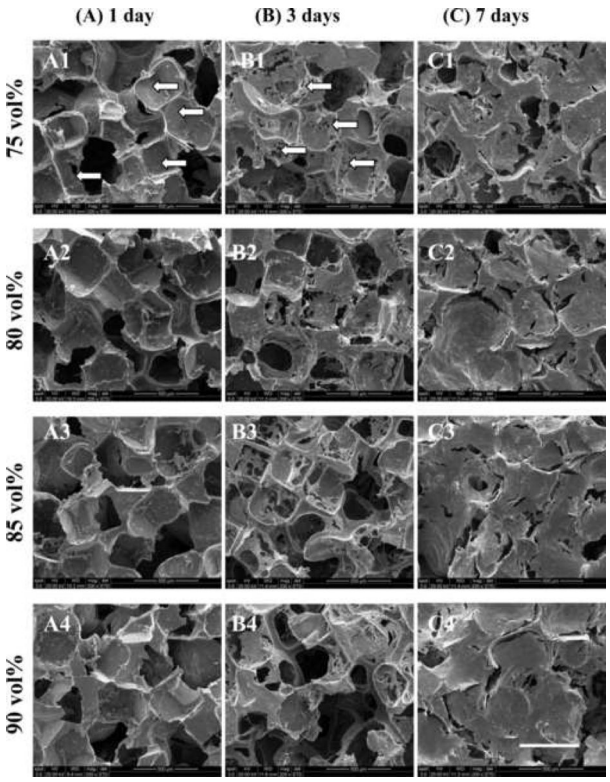

Figure 8.
SEM images of F-US-tube nanocomposite scaffolds with porogen fractions of 75, 80, 85, 90 vol % (from top to bottom) after seeding MSCs for (A1–4) 1 day, (B1–4) 3 days, and (C1–4) 7 days. Arrows indicate round-shaped (A1) or spread (B1) MSCs on the surface of scaffolds prepared with 75 vol% porogen. Scale bar represents 500 μm.

Table 1

Porosity of NaCl-leached scaffolds (mean ± standard deviation for n = 3).

Scaffold material	wt% NaCl at scaffold fabrication	vol% NaCl at scaffold fabrication	Porosity (%) by microCT	Porosity (%) by porosimetry
PPF	83.9	75.0	75.3 ± 2.3	76.5 ± 3.8
	87.4	80.0	80.5 ± 0.6	80.9 ± 1.0
	90.8	85.0	85.7 ± 0.7	84.1 ± 2.9
	94.0	90.0	90.4 ± 0.1	91.0 ± 2.4
US-tube nanocomposite	83.9	75.0	73.3 ± 2.6	74.0 ± 2.7
	87.4	80.0	78.9 ± 0.6	78.8 ± 3.0
	90.8	85.0	86.0 ± 0.9	84.1 ± 4.5
	94.0	90.0	89.6 ± 0.8	90.8 ± 3.2
F-US-tube nanocomposite	83.9	75.0	73.1 ± 0.8	73.1 ± 4.7
	87.4	80.0	78.6 ± 0.7	78.1 ± 3.6
	90.8	85.0	83.5 ± 1.1	84.0 ± 2.7
	94.0	90.0	90.7 ± 0.4	90.8 ± 1.0

Table 2

Interconnectivity of different scaffolds with 75–90 vol% porosities at various minimum connection sizes (mean ± standard deviation for n = 3).

Material	Porosity	Interconnectivity (%) at a minimum connection size						
		$20_{\mu m}$	$40_{\mu m}$	$60_{\mu m}$	$80_{\mu m}$	$100_{\mu m}$	$140_{\mu m}$	$200_{\mu m}$
PPF	75 vol%	99.3 ± 0.3	97.8 ± 1.1	94.9 ± 2.1	88.6 ± 4.3	77.9 ± 7.4	48.3 ± 12.2	21.0 ± 6.3
	80 vol%	99.5 ± 0.1	98.4 ± 0.2	96.1 ± 0.5	91.2 ± 1.0	83.2 ± 1.9	61.1 ± 3.0	27.3 ± 2.0
	85 vol%	99.6 ± 0.1	98.8 ± 0.2	97.3 ± 0.4	94.1 ± 1.0	88.5 ± 2.1	72.1 ± 4.5	36.0 ± 6.7
	90 vol%	99.8 ± 0.1	99.4 ± 0.1	98.6 ± 0.1	97.2 ± 0.3	94.9 ± 0.5	88.2 ± 1.0	69.3 ± 2.1
US-tube nanocomposite	75 vol%	99.3 ± 0.1	97.2 ± 0.6	91.8 ± 1.8	78.6 ± 5.0	56.5 ± 10.3	26.2 ± 10.7	13.1 ± 9.2
	80 vol%	99.3 ± 0.1	97.4 ± 0.3	94.1 ± 0.6	88.3 ± 1.1	78.1 ± 1.8	51.0 ± 4.0	19.2 ± 4.5
	85 vol%	99.5 ± 0.1	98.2 ± 0.3	95.2 ± 0.7	88.7 ± 1.6	81.9 ± 2.9	59.6 ± 5.2	28.2 ± 3.5
	90 vol%	99.5 ± 0.1	98.2 ± 0.3	95.5 ± 0.5	90.2 ± 0.9	87.1 ± 1.6	69.1 ± 3.0	39.7 ± 2.9
US-tube nanocomposite	75 vol%	99.7 ± 0.1	98.6 ± 0.1	96.3 ± 0.2	91.3 ± 0.4	82.2 ± 0.8	61.0 ± 2.8	30.0 ± 5.1
	80 vol%	99.7 ± 0.1	98.9 ± 0.2	97.5 ± 0.3	94.5 ± 0.6	87.6 ± 1.2	70.9 ± 2.4	53.8 ± 3.1
	85 vol%	99.7 ± 0.2	99.1 ± 0.7	97.9 ± 1.4	95.7 ± 2.0	91.8 ± 2.6	82.2 ± 3.5	66.9 ± 4.1
	90 vol%	99.8 ± 0.1	99.1 ± 0.1	98.0 ± 0.3	96.3 ± 0.5	94.3 ± 0.9	89.2 ± 1.6	75.4 ± 2.6